Quasiprojectile and intermediate velocity isotopic ratios for light fragments emitted in the ^{36}Ar + ^{58}Ni and ^{58}Ni + ^{58}Ni reactions between 32*A* and 84*A* MeV

J. Gauthier,[1] R. Roy,[1] P. St-Onge,[1] B. Wallace,[1] M. F. Rivet,[2] B. Borderie,[2] D. Gruyer,[3] J. D. Frankland,[3] A. Chbihi,[3] M. Boisjoli,[3] E. Legouee,[4] M. Pârlog,[4] R. Bougault,[4] N. Le Neindre,[4] P. Marini,[3] E. Rosato,[5] and D. Guinet[6]
(INDRA Collaboration)
[1]*Département de physique, de génie physique et d'optique, Université Laval, Québec, G1V 0A6, Canada*
[2]*Institut de Physique Nucléaire, IN2P3-CNRS, and Université Paris-Sud 11, 91406 Orsay, France*
[3]*GANIL, CEA-DSM/CNRS-IN2P3, Bvd. Henri Becquerel, F-14076 Caen Cedex, France*
[4]*LPC, CNRS/IN2P3, Ensicaen, Université de Caen, F-14050 Caen Cedex, France*
[5]*Istituto Nazionale di Fisica Nucleare, Sezione di Napoli, Complesso Universitario di Monte Sant'Angelo, I80126 Napoli, Italy*
[6]*Institut de Physique Nucléaire de Lyon, 69622 Villeurbanne Cedex, France*
(Received 5 October 2013; revised manuscript received 23 August 2014; published 22 September 2014; corrected 29 September 2014)

Isotopic ratios for light fragments ($Z \leqslant 4$) emitted by the quasiprojectile (QP) and the mid-rapidity (MR) sources are investigated by the use of a slightly asymmetric system (^{36}Ar + ^{58}Ni) and a symmetric one (^{58}Ni + ^{58}Ni) for six energies between 32*A* and 84*A* MeV and three semiperipheral centrality range selections. Experimental data come from the INDRA 4π multidetector. The results show a clear neutron-rich isotope production from the MR region as compared to the QP source. The beam energy and the centrality also show interesting different trends depending on the charge of the fragments and the emission source. Experimental results are compared to antisymmetrized molecular dynamics simulations.

DOI: 10.1103/PhysRevC.90.034618 PACS number(s): 25.70.−z

Heavy-ion reactions at intermediate energies offer a wide range of nuclear physics phenomena to study. From the most peripheral to the most violent collisions, many reaction processes have been observed and analyzed [1]. An interesting one among them is the formation of a third emission region between the projectile and the target occurring during peripheral and mid-peripheral collisions [2–4]. This nuclear matter grouping is called the mid-rapidity (MR) source and exhibits properties different from those of the excited quasiprojectile (QP). Recent investigations have shown that the heavier isotopes of light elements are preferentially emitted by the MR source [5–7] and the total N/Z ratio of this emitting region is higher than the N/Z of the QP [8–11]. Those phenomena may be caused by a proton migration induced by the Coulomb repulsion force and by the density dependence of the nuclear symmetry energy in this low-density region [12–14]. A recent study using symmetric and asymmetric systems at 25*A* MeV also shows a neutron enrichment for Li and Be fragments coming from the MR source and those results seem to be in agrement with isospin drift and diffusion processes [15].

In this work, we use a statistical identification method to evaluate the relative isotopic yield for fragments up to $Z = 4$ emitted by the MR source and the QP. These isotopic ratios are determined for a slightly asymmetric system (^{36}Ar + ^{58}Ni) and a symmetric one (^{58}Ni + ^{58}Ni) for six beam energies between 32*A* and 84*A* MeV and for three mid-peripheral centrality regions.

The experiments were performed at the Grand Accélérateur National d'Ions Lourds (GANIL) facility, France, and data were collected with the INDRA multidetector. The experimental setup has been previously described [16,17]. Here is a brief summary of INDRA features. INDRA is a set of 336 detection cells distributed on 17 rings covering 90% of the 4π solid angle. The detectors which make up the first ring are plastic scintillators in phoswich mode (a ring not used in this work). Rings 2 to 9 are made of three-stage detection modules. The first stage is an ionization chamber, followed by a silicon detector, and a CsI(Tl) scintillator. Rings 10 to 17 are composed of ionization chambers and CsI(Tl) but, for ^{36}Ar + ^{58}Ni, ionization chambers were not installed on rings above 12. This setup provides charge identification up to $Z = 54$ for a $3^\circ \leqslant \theta_{\rm lab} \leqslant 45^\circ$ angular range and up to $Z = 16$ for $45^\circ \leqslant \theta_{\rm lab} \leqslant 176^\circ$ in the case of ^{58}Ni + ^{58}Ni. For ^{36}Ar + ^{58}Ni, only fragments up to $Z = 4$ are identified above 90°. Isotopic identification up to $Z = 4$ is achieved below 90° for fragments having a reduced rapidity (parallel velocity divided by the initial projectile rapidity) higher than 0.5. Beam energies are 32*A*, 40*A*, 52*A*, 63*A*, 74*A*, and 84*A* MeV for ^{36}Ar + ^{58}Ni and 32*A*, 40*A*, 52*A*, 64*A*, 74*A*, and 82*A* MeV for ^{58}Ni + ^{58}Ni. During the data acquisition, the multiplicity threshold was set to 3 for ^{36}Ar + ^{58}Ni from 32*A* to 63*A* MeV and to 4 for all the other reactions.

The first step of this analysis consists of selecting complete events. For this purpose, we use the pseudomomentum global variable defined by

$$\text{pseudo}P = \sum_{i=1}^{M} Z_i V_{||}^i. \quad (1)$$

Here, M is the event multiplicity, Z_i is the charge of particle i, and $V_{||}^i$ is the parallel velocity of that particle. Since only fragments with velocity higher than half the velocity of the projectile are taken into account, the minimum total detected charge must be close to the charge of the projectile. So, events with a pseudo$P$ value higher than 70% of $V_{\rm proj}Z_{\rm proj}$ are selected. Figure 1 shows an example of this selection for the asymmetric system ^{36}Ar + ^{58}Ni at 40*A* MeV.

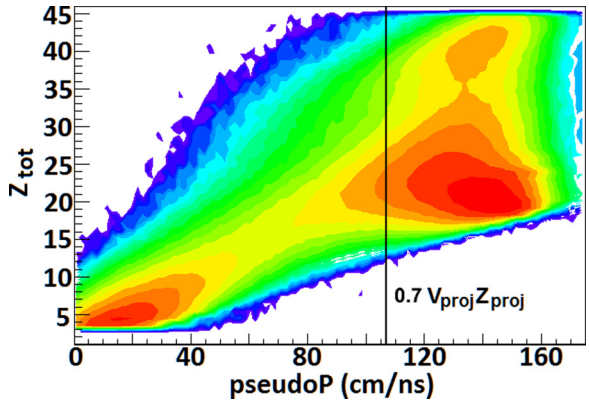

FIG. 1. (Color online) Total charge as a function of the pseudo-momentum for the ^{36}Ar + ^{58}Ni reaction at 40*A* MeV.

In order to define centrality regions, a variable sensitive to the impact parameter is used. A well-correlated global variable with the centrality previously used [7,18,19] is the total transverse energy $E^{\rm tot}_{\rm trans}$ as described in

$$E^{\rm tot}_{\rm trans} = \sum_{i=1}^{M} E^{i}_{\rm lab} \sin^2\left(\theta^{i}_{\rm lab}\right). \tag{2}$$

$E^{i}_{\rm lab}$ and $\theta^{i}_{\rm lab}$ are the energy and the polar angle, respectively, of particle i in the laboratory frame of reference. Since this variable represents the transverse component of the total energy detected after a collision, the centrality is statistically proportional to its value with few fluctuations. For the purpose of this work, the $E^{\rm tot}_{\rm trans}$ variable is utilized to construct an empirical experimental impact parameter denoted $b_{\rm exp}$. This parameter is described in

$$b_{\rm exp} = b_{\rm max}\left[1 - C\left(\frac{E^{\rm tot}_{\rm trans}}{E_{\rm proj}}\right)\right]. \tag{3}$$

Here, C is a constant with an empirically set value equal to 3.14, and we define $b_{\rm max}$ as

$$b_{\rm max} = 1.2\left(A^{1/3}_{\rm proj} + A^{1/3}_{\rm target}\right). \tag{4}$$

It should also be noticed that $E_{\rm proj}$ is the laboratory kinetic energy of the projectile and A is the mass number.

We used the event generator HIPSE (Heavy Ion Phase Space Exploration) [20] to evaluate the correlation between $b_{\rm exp}$ and b. Figure 2(a) shows $b_{\rm exp}$ as a function of the impact parameter b generated by using HIPSE for the ^{36}Ar + ^{58}Ni at 52*A* MeV simulated reaction. In the case of peripheral and mid-peripheral collisions ($b_{\rm exp} > 6$), a Gaussian fit performed on the $b_{\rm exp\_cor} - b$ distribution gives a standard deviation equal to 0.55 fm. Here, $b_{\rm exp\_cor}$ is $b_{\rm exp}$ corrected by a linear fit performed on the $b(b_{\rm exp})$ distribution [Fig. 2(a)]. In the case of Fig. 2(b), $b_{\rm exp\_cor} = 0.84 b_{\rm exp}$.

Wanting to study the effect of centrality with good precision, we chose intervals of 0.5 fm. We can observe the variation of centrality effects from one delimited region to the other. This confirms our choice of interval as being adequate. Using the experimental impact parameter gives rise to a statistical distribution and so to a certain overlap of the effect from one region to the other [18]. Figure 3 presents the three $b_{\rm exp}$ intervals chosen for each system. These intervals are 6–6.5, 6.5–7, and 7–7.5 fm for ^{36}Ar + ^{58}Ni. Since $b_{\rm max}$ is higher for ^{58}Ni + ^{58}Ni, the intervals are shifted by a value of 0.5 fm for this system.

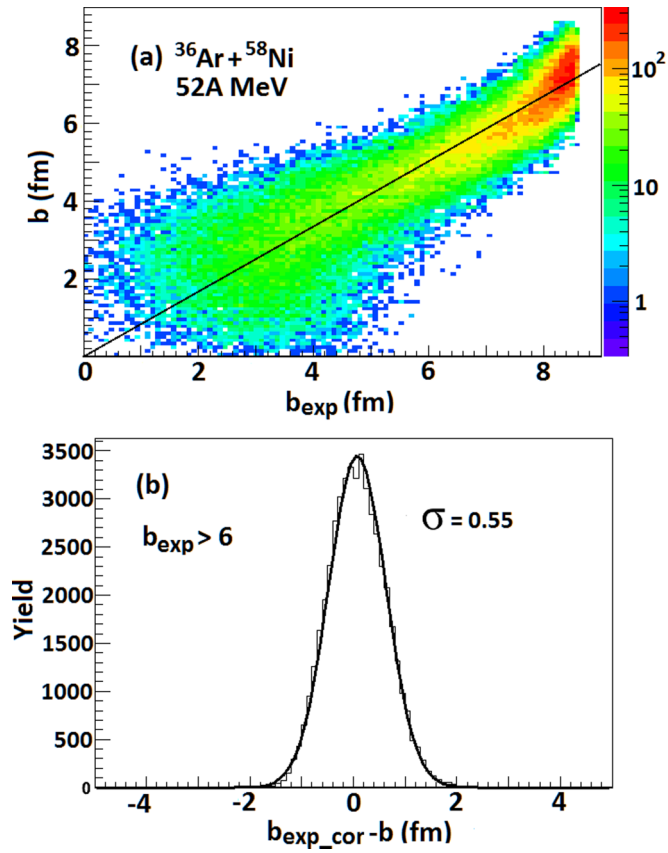

FIG. 2. (Color online) (a) b as a function of $b_{\rm exp}$ for the ^{36}Ar + ^{58}Ni reaction at 52*A* MeV simulated by using HIPSE (no filter). (b) Gaussian fit on the $b_{\rm exp} - b$ distribution.

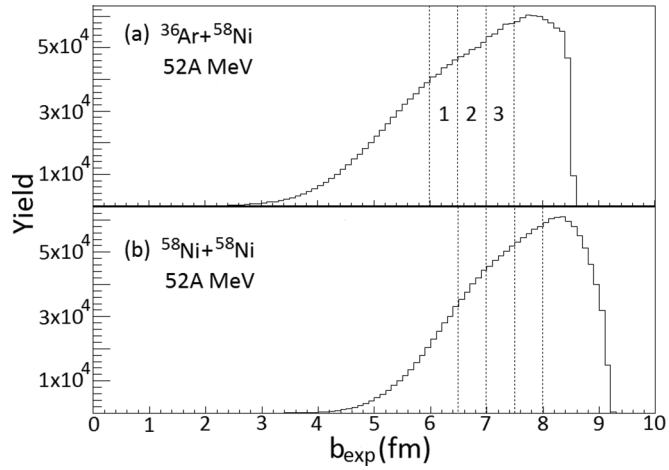

FIG. 3. The three selected regions of the experimental impact parameter ($b_{\rm exp}$) for ^{36}Ar + ^{58}Ni (a) and ^{58}Ni + ^{58}Ni (b) reactions at 52*A* MeV.

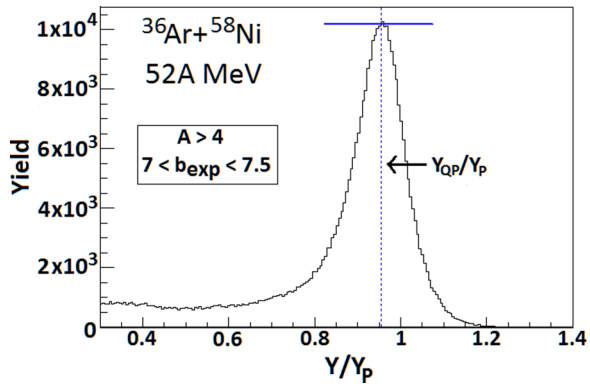

FIG. 4. (Color online) Estimation of the QP rapidity for ^{36}Ar + ^{58}Ni at 52A MeV. See text for details.

The emission sources are identified by using the statistical method called EVAP in Ref. [7]. We first have to evaluate the mean QP reduced rapidity. This is done by making an inverted Maxwell fit on the reduced rapidity distribution for $A > 4$ fragments in order to define the highest yield of the peak, as shown in Fig. 4. The reduced rapidity corresponding to the top of this peak represents the QP rapidity estimation.

By assuming that all light particles emitted above this value are coming from this source and that the statistical emission of those particles is symmetric along the perpendicular axes to the beam in the QP frame, the backward emission is deduced by symmetrizing the forward distribution toward the back from the QP rapidity. Instead of simply calculating integrals and subtracting distributions, probability tables are constructed [21], based on the forward QP emission distributions for each $Z < 5$ isotope. These tables allow us to allocate particles to the QP and the MR emission sources while keeping available complete information about these particles. Figure 5 shows the result of the method applied to α particles produced in the ^{36}Ar + ^{58}Ni reaction at 52A MeV in the 7–7.5 $b_{\rm exp}$ interval. The "Mass_ID=0" region corresponds to unresolved helium masses. Since the mass identification is not completely achieved for $Z < 5$ fragments below $V_{||}/V_p = 0.5$, we only take into account fragments having a reduced rapidity higher

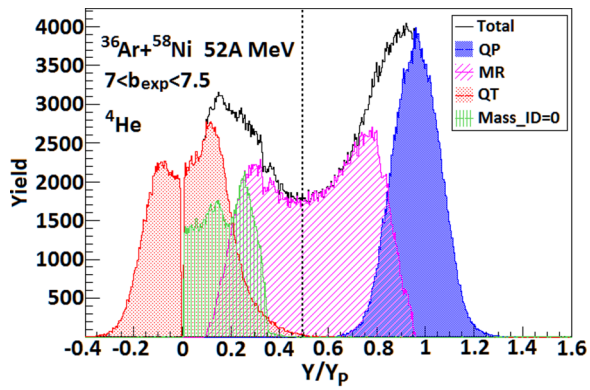

FIG. 5. (Color online) ^{4}He source selection by using the statistical method for ^{36}Ar + ^{58}Ni at 52A MeV in the $7 < b_{\rm exp} < 7.5$ region. The "Mass_ID=0" region corresponds to unresolved masses.

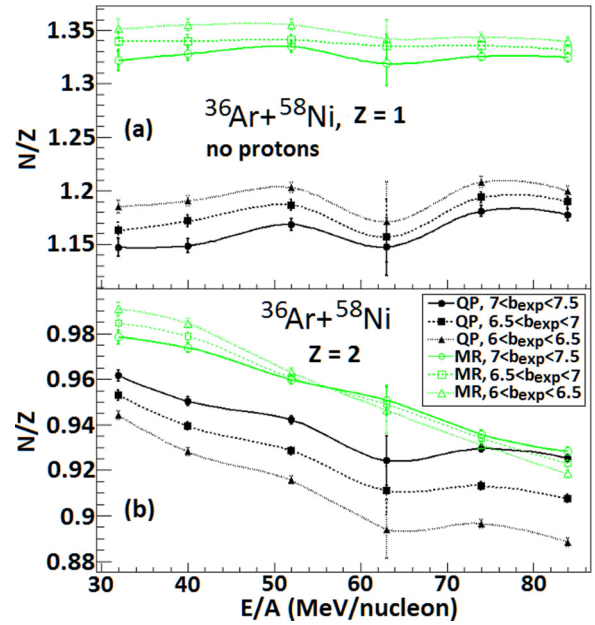

FIG. 6. (Color online) Experimental N/Z of H (a) and He (b) isotopes as a function of the beam energy for ^{36}Ar + ^{58}Ni. Closed (open) symbols correspond to the QP (MR source). The three selected centrality regions are also shown. ^{1}H results are not included. Lines serve to guide the eye.

than 0.5. The experimental N/Z ratios calculated by using the method described above for light particles ($Z \leqslant 2$) are shown in Fig. 6 for ^{36}Ar + ^{58}Ni and in Fig. 7 for ^{58}Ni + ^{58}Ni.

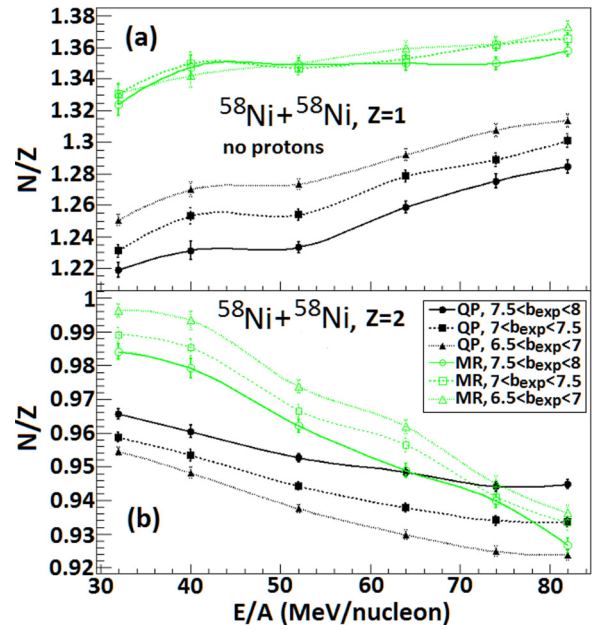

FIG. 7. (Color online) Experimental N/Z of H (a) and He (b) isotopes as a function of the beam energy for ^{58}Ni + ^{58}Ni. Closed (open) symbols correspond to the QP (MR source). The three selected centrality regions are also shown. ^{1}H results are not included. Lines serve to guide the eye.

Since systematic error generated by using the EVAP method is very hard (even impossible) to evaluate [7] and this analysis treats only mean values, only statistical error is shown on the graphs. However, a systematic error is added to the statistical error bars on ^{36}Ar + ^{58}Ni points at 63*A* MeV to take into account an instrumental problem that occurred during the experiment. A temperature instability in the CsI(Tl) crystals at the beginning of the 63*A* MeV run led to some particle identification uncertainties. This is why the error bars are larger at this energy. Also, since the overlap between the emission sources is very high for protons, the statistical method highly overestimates the contribution of the QP for these particles. Moreover, free neutrons are not detected by INDRA. For those reasons, free protons are not included in hydrogen N/Z ratios.

The N/Z ratios of light particles are always higher for the MR source except at the highest energy for $Z = 2$. The point corresponding to the highest b_{exp} interval applied to the QP for helium isotopes crosses the MR points for ^{36}Ar + ^{58}Ni and this overlap is even stronger for ^{58}Ni + ^{58}Ni. This can be explained by the fact that the ^{3}He yield increases almost linearly with the beam energy for the two sources but the slope is higher for the MR source. That leads to a faster drop of N/Z as a function of the energy for the MR source as compared to the QP. The global trends are very similar for the two systems. About $Z = 1$, the N/Z ratios stay pretty much constant as a function of the energy for ^{36}Ar + ^{58}Ni. In the case of the symmetric system, the gap between the sources seems to decrease for $Z = 1$. This behavior could be caused by an increase of ^{3}H production inside the QP as a function of the energy. Since the ^{58}Ni projectile is heavier and has a slightly higher N/Z than ^{36}Ar, this effect would be then more apparent for the ^{58}Ni + ^{58}Ni system. Another interesting behavior concerns the centrality selection. The QP is clearly more sensitive to this parameter than the MR source. It is normal to observe an increase in the N/Z ratios for a smaller impact parameter for $Z = 1$, 3, and 4 particles because the isotopic distributions should become broader on the neutron side with the violence of collisions. However, the opposite is expected for $Z = 2$ particles, as seen in Fig. 7, since more ^{3}He particles are produced with increasing energy and collision violence [22], so that the ratios decrease accordingly for those particles. This is another confirmation that the particles coming from the MR source are generated mostly by dynamical processes instead of statistical decays following a thermal equilibrium state.

Figures 8 and 9 show the results for $Z = 3$ and $Z = 4$, respectively. Since the identification of ^{8}Be is difficult and introduces a statistical bias in the velocity distributions, this isotope is not included in the ratios. Again, the N/Z ratios are generally higher for the MR source except for $Z = 4$ generated by ^{36}Ar + ^{58}Ni above 52*A* MeV. The trend is similar for ^{58}Ni + ^{58}Ni but the gap between sources is significant for all beam energies. The centrality effect on the MR source and the QP is similar for $Z = 3$ and $Z = 1$. However, it has almost no effect on the QP for $Z = 4$. This could suggest a significant difference between light particles and heavier fragment formation and emission processes for the two sources. Globally, the N/Z ratio is constant or increases with energy but decreases for both sources in the case of $Z = 2$

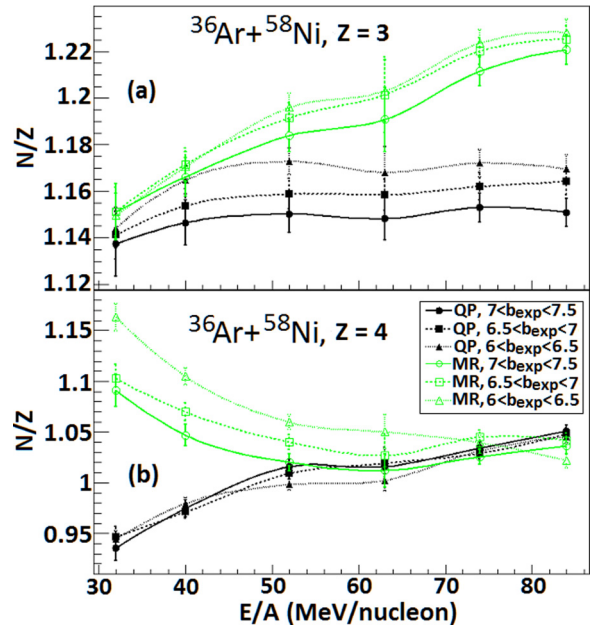

FIG. 8. (Color online) Experimental N/Z of Li (a) and Be (b) isotopes as a function of the beam energy for ^{36}Ar + ^{58}Ni. Closed (open) symbols correspond to the QP (MR source). The three selected centrality regions are also shown. ^{8}Be results are not included. Lines serve to guide the eye.

and for the MR source in the case of $Z = 4$. As mentioned above, the increase of the ^{3}He emission rate as a function of the reaction energy can explain this trend for $Z = 2$. For

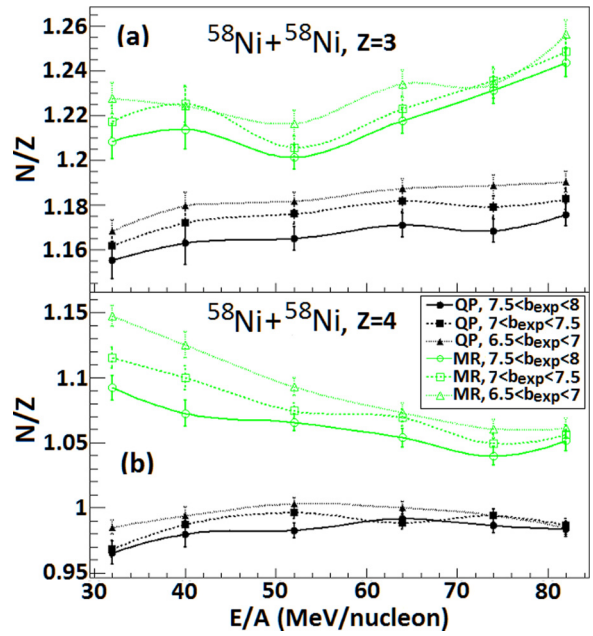

FIG. 9. (Color online) Experimental N/Z of Li (a) and Be (b) isotopes as a function of the beam energy for ^{58}Ni + ^{58}Ni. Closed (open) symbols correspond to the QP (MR source). The three selected centrality regions are also shown. ^{8}Be results are not included. Lines serve to guide the eye.

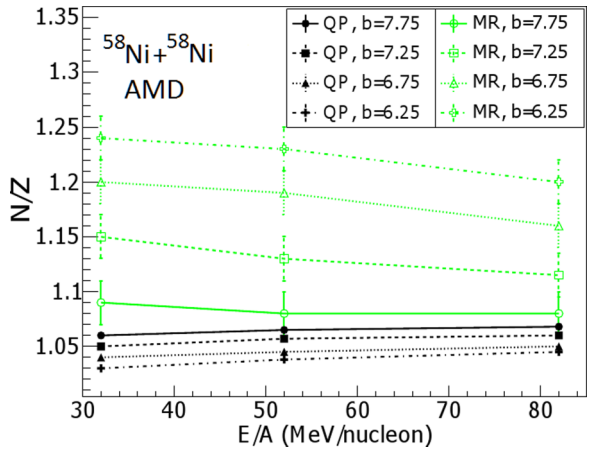

FIG. 10. (Color online) Total N/Z ratio as a function of the energy of the ^{58}Ni + ^{58}Ni reaction at 32A, 52A, and 82A MeV simulated by using AMD (no filter). Closed (open) symbols correspond to the QP (MR source). Four centrality regions are also shown. Lines serve to guide the eye.

$Z = 4$, the isotopic ratios calculated during this analysis [23] show that the ^{7}Be percentage increases with energy while the ^{9}Be one decreases for the MR source. The ^{10}Be percentage, on the other hand, follows a trend similar to that of the overall $Z = 4$ N/Z ratio. This is why the MR N/Z ratio decreases with energy for beryllium. This behavior cannot be explained by a bad identification at low velocity since the isotopic resolution for $Z = 4$ (excluding ^{8}Be) is completely achieved above $V_{||}/V_{\text{proj}} = 0.6$ for 32A MeV and above 0.5 for 40A MeV. Also, the inclusion of ^{8}Be would modify the trend by moving the N/Z value toward 1 but, as mentioned above, adding this isotope would introduce a more important bias than its exclusion. It should be noticed that the overall trend for ^{58}Ni + ^{58}Ni at 52A and 74A MeV is in agreement with the experimental results presented in Ref. [24], i.e., a higher N/Z ratio for $Z \leqslant 4$ MR fragments and a slightly more important effect of the centrality parameter on this ratio for the QP.

Antisymmetrized molecular dynamics (AMD) simulations [25,26] of a large amount of events (200 000 for each impact parameter value) of the ^{58}Ni + ^{58}Ni reaction at 32A, 52A, and 82A MeV show a higher overall N/Z ratio for the MR source compared to that of the QP. Figure 10 presents those results. The simulation is stopped at 205 fm/c. The source separation is achieved by a technique similar to the one described above, except that it makes use of the positions of the nucleons upon the beam axis instead of their parallel velocity. A complex statistical Gaussian fit [27] is performed to separate the QP and quasitarget sources from the MR and pre-equilibrium sources. The source overlap is then weak and they are well separated. A symmetrization of the forward QP emission is made toward the back of the peak and the rest of the distribution is assigned to the MR source contribution. The N/Z ratios are calculated from the nucleons present in the selected zones, without attempt to build clusters. The centrality parameters have been selected according to the corrected b_{exp} based on HIPSE simulations in order to compare results with the experimental trends shown above. Impact parameters are fixed values separated by 0.5 fm situated in the middle of each experimental centrality regions in order to compare with experimental analysis. From Fig. 10, we can see that the overall MR N/Z ratio is always higher than the QP one and 0.5 fm centrality separation generates statistical differences between values. Since the MR neutron enrichment (and thus the QP impoverishment since more neutrons in the MR source means fewer in the two other sources due to the mirror effect) is a function of the number of interacting nucleons, the MR N/Z ratio should increase according to the centrality and decrease with the beam energy, and this is the behavior that we observe from the simulations. The higher N/Z ratio for the MR source is also in agreement with our experimental results. Moreover, the energy and centrality trends are very similar to those observed experimentally for $Z = 4$ isotopes (see Fig. 9). We saw in experimental results that the impact parameter value has a greater effect on QP N/Z than on that of the MR source except for $Z = 4$ where the trend is inverted. This is the exact behavior of our AMD simulated overall N/Z and this is expected because heavy fragment samples contain more nucleons and are then closer to the overall neutron-to-proton ratio.

We have presented one of the most complete isotopic study of fragments up to $Z = 4$ emitted by the MR and the QP sources so far using INDRA data for ^{36}Ar + ^{58}Ni and ^{58}Ni + ^{58}Ni between 32A and 84A MeV. The source identification has been made by using the statistical method combined with probability tables. The N/Z ratio of each element is generally higher for the MR source. Also, the centrality seems to have a greater effect on the QP as compared to the MR source for light particles, but this trend is inverted for heavier fragments. Furthermore, AMD simulations show clearly an overall neutron enrichment of the MR source, which is in agreement with our measurements, especially for $Z = 4$. Those results suggest that the isotope formation mechanisms are different for light particles than for light fragments and also strongly depend on the nature of the emission source. A similar study with a higher isotopic resolution could give more complete information about the intermediate mass fragment isotopic formation inside the MR region.

We wish to acknowledge the INDRA Collaboration and GANIL for making this work possible as well as the Natural Sciences and Engineering Research Council of Canada for support of the Université Laval heavy-ion research group. AMD simulations have been made possible through access to the supercomputing facilities of CLUMEQ, Compute Canada.

[1] B. Borderie and M. F. Rivet, Prog. Part. Nucl. Phys. **61**, 551 (2008).
[2] C. P. Montoya *et al.*, Phys. Rev. Lett. **73**, 3070 (1994).
[3] J. Lukasik *et al.*, Phys. Rev. C **55**, 1906 (1997).

[4] M. Di Toro *et al.*, Eur. Phys. J. A **30**, 65 (2006).
[5] E. Plagnol *et al.* (INDRA Collaboration), Phys. Rev. C **61**, 014606 (1999).
[6] Y. Larochelle *et al.*, Phys. Rev. C **62**, 051602(R) (2000).
[7] T. Lefort *et al.*, Nucl. Phys. A **662**, 397 (2000).
[8] D. Thériault *et al.*, Phys. Rev. C **71**, 014610 (2005).
[9] D. Thériault *et al.* Phys. Rev. C **74**, 051602(R) (2006).
[10] Z. Kohley *et al.*, Phys. Rev. C **83**, 044601 (2011).
[11] E. De Filippo *et al.*, Phys. Rev. C **86**, 014610 (2012).
[12] M. Larivière Bastien, Master's thesis, Université Laval, 2009.
[13] M. Colonna, M. Di Toro, G. Fabbri, and S. Maccarone, Phys. Rev. C **57**, 1410 (1998).
[14] B.-A. Li, L.-W. Chen, H.-R. Ma, J. Xu, and G.-C. Yong, Phys. Rev. C **76**, 051601(R) (2007).
[15] I. Lombardo *et al.*, Phys. Rev. C **82**, 014608 (2010).
[16] J. Pouthas *et al.*, Nucl. Instrum. Methods A **357**, 418 (1995).
[17] J. Pouthas *et al.*, Nucl. Instrum. Methods A **369**, 222 (1996).
[18] J. Péter *et al.*, Nucl. Phys. A **519**, 611 (1990).
[19] J. D. Frankland *et al.* (INDRA Collaboration), Nucl. Phys. A **689**, 905 (2001).
[20] D. Lacroix, A. Van Lauwe, and D. Durand, Phys. Rev. C **69**, 054604 (2004).
[21] L. Gingras *et al.*, Phys. Rev. C **65**, 061604(R) (2002).
[22] B. V. Jacak *et al.*, Phys. Rev. C **35**, 1751 (1987).
[23] J. Gauthier, Ph.D. thesis, Université Laval, 2012.
[24] E. Galichet, M. Colonna, B. Borderie, and M. F. Rivet, Phys. Rev. C **79**, 064615 (2009).
[25] A. Ono and H. Horiuchi, Prog. Part. Nucl. Phys. **53**, 501 (2004).
[26] A. Ono, Phys. Rev. C **59**, 853 (1999).
[27] B. Wallace, EPJ Web Conf. **66**, 10018 (2014).